

Domain- and symmetry-transition origins of reduced nanosecond piezoelectricity in ferroelectric/dielectric superlattices

This article has been downloaded from IOPscience. Please scroll down to see the full text article.

2012 New J. Phys. 14 013034

(<http://iopscience.iop.org/1367-2630/14/1/013034>)

View [the table of contents for this issue](#), or go to the [journal homepage](#) for more

Download details:

IP Address: 128.104.200.177

The article was downloaded on 19/01/2012 at 14:34

Please note that [terms and conditions apply](#).

Domain- and symmetry-transition origins of reduced nanosecond piezoelectricity in ferroelectric/dielectric superlattices

Pice Chen^{1,5}, Ji Young Jo^{1,4,5}, Ho Nyung Lee², Eric M Dufresne³, Serge M Nakhmanson³ and Paul G Evans^{1,6}

¹ Department of Materials Science and Engineering and Materials Science Program, University of Wisconsin, Madison, WI 53706, USA

² Materials Science and Technology Division, Oak Ridge National Laboratory, Oak Ridge, TN 37831, USA

³ Argonne National Laboratory, Argonne, IL 60439, USA

⁴ School of Materials Science and Engineering, Gwangju Institute of Science and Technology, Gwangju 500-712, Korea

E-mail: evans@engr.wisc.edu

New Journal of Physics **14** (2012) 013034 (12pp)

Received 11 October 2011

Published 18 January 2012

Online at <http://www.njp.org/>

doi:10.1088/1367-2630/14/1/013034

Abstract. Complex-oxide superlattices (SLs) with atomic-scale periodicity have dynamical properties that are distinct from thin films of uniform composition. The origins of these properties are closely related to the dynamics of polarization domains and to field-driven changes in the symmetries resulting from interfacial coupling between different components. These dynamics are apparent at timescales from a few nanoseconds to several milliseconds in experiments probing the piezoelectricity of a ferroelectric/dielectric BaTiO₃(BTO)/CaTiO₃ (CTO) SL using time-resolved x-ray microdiffraction. At the 100 ns timescale, the piezoelectric distortion is approximately ten times smaller than in the millisecond regime. This reduced piezoelectricity at short timescales is not observed in previously studied PbTiO₃/SrTiO₃ SLs or compositionally uniform ferroelectrics such as tetragonal compositions of Pb(Zr, Ti)O₃. The unusual behavior of the BTO/CTO SL can be linked to the switching of a nanodomain state into a uniform polarization state or to a field-induced crystallographic symmetry transition. A comparison of the results

⁵ These authors have contributed equally to this work.

⁶ Author to whom any correspondence should be addressed.

with the characteristic timescales of these two dynamical phenomena in other complex oxides with different compositions suggests that the phase transition is a more likely possibility.

Contents

1. Introduction	2
2. Millisecond- and nanosecond-duration time-resolved x-ray microdiffraction	4
3. Structural and electrical evidence for intermediate-timescale dynamics in BaTiO₃/CaTiO₃ superlattices	5
4. Scaling of strain with the applied electric field	7
5. Origins of reduced piezoelectricity	10
6. Conclusion	11
Acknowledgments	11
References	11

1. Introduction

Ferroelectric/dielectric superlattices (SLs) promise to enable precise control over the electronic and structural properties of complex-oxide electronic materials through the use of the coupling of structural, chemical and electronic degrees of freedom between compositionally distinct layers. Internal electric fields and structural parameters including strain and octahedral tilts in distinct layers of the SL can interact to yield intriguing properties such as the continuity of electrical polarization through layers of different compositions [1–3], the formation of striped domains with well-defined periodicities [4–6] and the modification of ferroelectricity in the ground state [7]. These phenomena and the resulting intriguing materials properties are sensitive to external perturbations, resulting in fascinating dynamical phenomena. For example, the dynamics of the domain switching and phase transitions induced by applied electric fields provide insight into the coupling of nanoscale domain phenomena, polarization and collective distortion of the crystallographic structure. Research activities so far, however, have largely been focused on the properties of SLs near equilibrium. Dynamical phenomena in SLs are only beginning to be investigated [5, 6].

In SL systems where polarization domains have well-defined striped periodicities, the time dependence and kinetic processes of domain switching have been probed directly using the structural modulation coupled to the periodic polarization [4, 6]. This approach is limited to SLs where well-defined striped domains are formed, such as PbTiO₃(PTO)/SrTiO₃ (STO) SLs. The electric-field-induced heterogeneous transition from the striped-domain state to a uniform polarization state in the PTO/STO system has a large effect on the piezoelectric distortion of the lattice. The characteristic time of this domain-switching transition depends on the magnitude of the applied electric field, and can be as short as a few nanoseconds [6]. In SLs with different compositions, a more randomized domain pattern has been reported [8]. The dynamical consequences of a non-periodic domain structure, however, remain unclear.

In addition to the largely mesoscopic effects associated with polarization domains, a second atomic-scale set of phenomena arises from field-induced modifications of the crystallographic symmetry. Bulk forms of the components of SLs can exhibit several different crystallographic

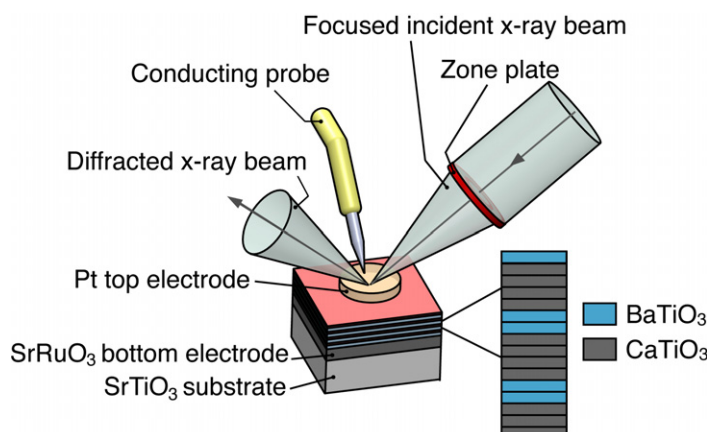


Figure 1. Time-resolved x-ray microdiffraction. The layer structure of the BTO/CTO SL is shown in the inset.

motifs in their ground states, including antiferrodistortive and ferroelectric order [7, 9]. The competition between these structural effects in SLs plays a key role in determining the equilibrium crystallographic symmetry and has a strong influence on ferroelectric properties [7, 10]. Both the direction and magnitude of polarization in SL are hypothesized to be susceptible to field-induced transitions between antiferrodistortive symmetries and more highly polar ferroelectric states [11–13]. These field-induced symmetry transitions are conceptually similar to those in relaxor ferroelectrics, ferroic materials near a morphotropic phase boundary and ferroelectrics governed by the polarization–rotation mechanism [14, 15], in that the electric field can be sufficient to move the system between the states with different symmetries. Field-induced antiferroelectric-to-ferroelectric transitions are commonly found [16], and the interesting case of stress-mediated ferroelectric-to-antiferroelectric transitions has recently been reported in PbZrO_3 -based ceramics [17, 18]. Little is known about the associated dynamics of these structural transitions.

The time dependence of the piezoelectricity of BaTiO_3 (BTO)/ CaTiO_3 (CTO) SLs provides insights into the dynamical phenomena associated with competing structural and electronic effects. The component compounds have well-defined structural ordering, including ferroelectric order in BTO and antiferrodistortive order in CTO [19]. The interaction of these structural phenomena defines the ground state of BTO/CTO SLs [12]. Here we show that the maximum piezoelectric strain of a BTO/CTO SL measured during nanosecond-duration electric pulses is much smaller than that in millisecond-duration electric fields, regardless of the magnitude of electric fields. This difference in piezoelectric distortion at nanosecond timescales has not been found in structural studies of conventional ferroelectrics [20] or in PTO/STO SLs [6]. The reduced piezoelectricity at the nanosecond timescale and the microsecond-scale decay of the stored polarization are evidence of slow dynamical processes occurring at an intermediate characteristic time. The related dynamical phenomena can include the switching of polarization nanodomains or field-induced crystallographic symmetry transitions.

The BTO/CTO SL for this study was grown by pulsed laser deposition on a SrRuO_3 (SRO) conducting bottom electrode on a (001)-oriented STO substrate [21]. The SL has a nominal repeating unit consisting of 2 unit cells of BTO and 4 unit cells of CTO (figure 1, inset) with an overall thickness of 200 nm. Platinum top electrodes with a diameter of $100\ \mu\text{m}$ were deposited

on top of the SL to form thin-film capacitors. The out-of-plane lattice constant of the SL varies across the surface of the sample due to local structural variations, as is apparent in the 0.06% difference in steady-state lattice constants for the two different capacitors compared in the short- and long-timescale measurements described below. X-ray reflections from the SL appear at values of q_z that satisfy [12]

$$q_z = \frac{2\pi}{t_{\text{avg}}} \left(m + \frac{l}{n} \right).$$

Here t_{avg} is the average lattice constant of the SL, m is a positive integer corresponding to the index of the Bragg reflection of the average spacing, n is the number of unit cells in each repeating unit and l is an integer labeling satellites arising from the SL periodicity. The average repeating unit was experimentally found to have $n = 6.6$ unit cells due to variations in the layer thicknesses in either the BTO or CTO component [17]. Here we focus on the dynamics of the $m = 2$ $l = 0$ SL reflection, which corresponds to the (002) Bragg reflection of the average SL atomic spacing, which varies from 3.984 to 3.986 Å. We have previously reported a piezoelectric coefficient of 54 pm V⁻¹ for these SLs [11, 12], and we have found that this value also varies across the sample, as is illustrated below.

2. Millisecond- and nanosecond-duration time-resolved x-ray microdiffraction

Time-resolved x-ray microdiffraction studies of the BTO/CTO SL were conducted at the Advanced Photon Source (APS) using the experimental arrangement shown in figure 1. Incident x-rays with a photon energy of 10 keV were focused by a Fresnel zone plate to a 250–300 nm spot located within the capacitors. Long-timescale experiments with a time resolution of 50 μ s were conducted at the APS station 7-IDC [12]. Millisecond-duration electric field waveforms were applied across the thickness of the SL capacitor by using a tungsten probe tip to contact the top electrode (figure 1). The diffracted beam was detected using an avalanche photodiode (APD). The triangle-waveform electric fields had a duration of 2.5 ms and a magnitude of 20 V, nominally equivalent to an electric field of 1 MV cm⁻¹. The arrival times of the pulses from the APD were sorted using a multichannel scaler (MCS) synchronized to the applied electric fields. The MCS counted diffracted x-ray photons in 100 channels with a dwell time of 50 μ s per channel.

A second series of measurements with nanosecond time resolution were carried out at station 7-IDB of the APS. In this case, electric fields were supplied by a pulse generator capable of producing pulses with sub-nanosecond rise times. Electrical pulses corresponding to photons detected by the APD were gated by digital electronics to select photons scattered from x-ray bunches with the desired time relationship to the applied electric field. Electric-field pulses were separated by intervals of 73 μ s, synchronized with the beam rotation clock of the APS storage ring, yielding an electric-field pulse repetition rate of approximately 14 kHz. In these nanosecond-resolution measurements, the scans proceeded by positioning the diffractometer at a series of angles corresponding to each point in reciprocal space and then measuring the intensity at a series of delay times. At each time point, the data acquisition consisted of 5000 (figures 2, 4 and 5) or 9999 (figure 7) repetitions of the electric field pulses in order to achieve sufficient counting statistics. We expect each repetition of the pump–probe measurement to be independent because the 73 μ s interval between electric field pulses is similar to the polarization decay time observed in the electrical measurements illustrated below. The nanosecond time

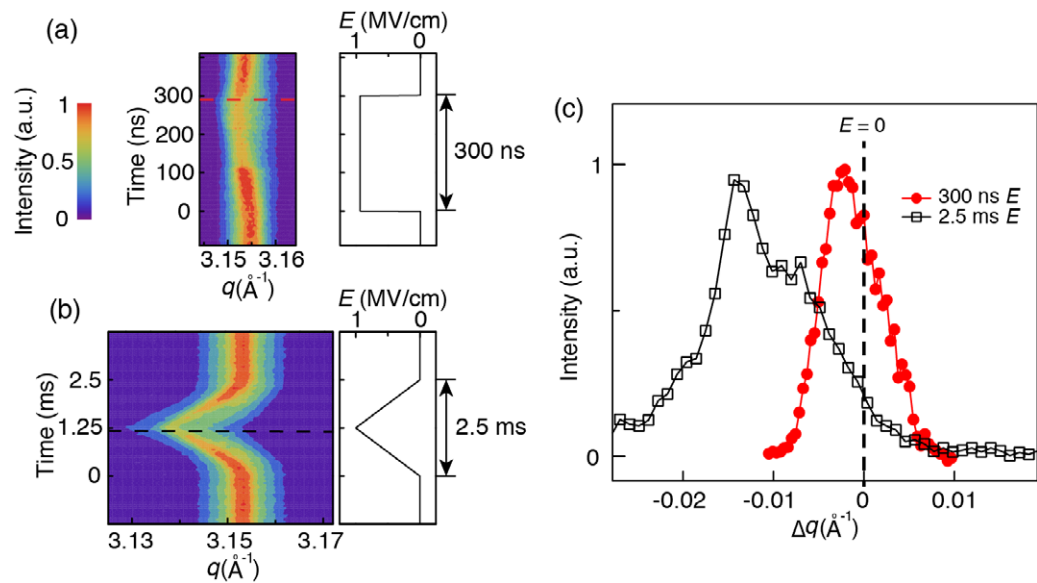


Figure 2. Intensities near the $m = 2$ $l = 0$ x-ray reflections of the BTO/CTO SL as a function of the elapsed time and wavevector q_z during (a) 300 ns electric field pulses and (b) 2.5 ms triangle-wave electric fields. The intensity scale is normalized to the peak intensity in each plot. Electric field waveforms are shown to the right of the plots. (c) $m = 2$ $l = 0$ diffraction patterns acquired at an elapsed time of 291 ns in the plot shown in (a) (circles) and at 1.2 ms in the plot shown in (b) (squares). The electric fields are 0.94 and 0.96 MV cm⁻¹, respectively. The line at $\Delta q = 0$ indicates the wavevector of maximum intensity at zero electric field.

resolution of these experiments is much longer than the 100 ps timescales associated with mechanical resonances of the total thickness of the SL thin film.

The 300 ns duration of the electric field in the pulsed measurements was greater than the 153 ns interval between x-ray bunches in the operating mode of the APS used in this study. In order to speed up the data acquisition, the experimental circuitry recorded the intensities from three sequential x-ray bunches and thus three diffraction patterns simultaneously at three different time points separated by 153 ns. Overlapping time points resulting from the use of the series of x-ray bunches appear in the data and serve as a measure of the reproducibility of the measurement.

3. Structural and electrical evidence for intermediate-timescale dynamics in BaTiO₃/CaTiO₃ superlattices

The dynamics of the piezoelectric expansion of the SLs in applied electric fields is closely related to the associated structural distortions and electrical properties such as the stored polarization. Figure 2(a) shows the distribution of diffracted intensity near the $m = 2$ $l = 0$ SL reflection as a function of time during 300 ns electric field pulses with a magnitude of 0.94 MV cm⁻¹. The peak intensity of the SL x-ray reflection shifts monotonically to lower

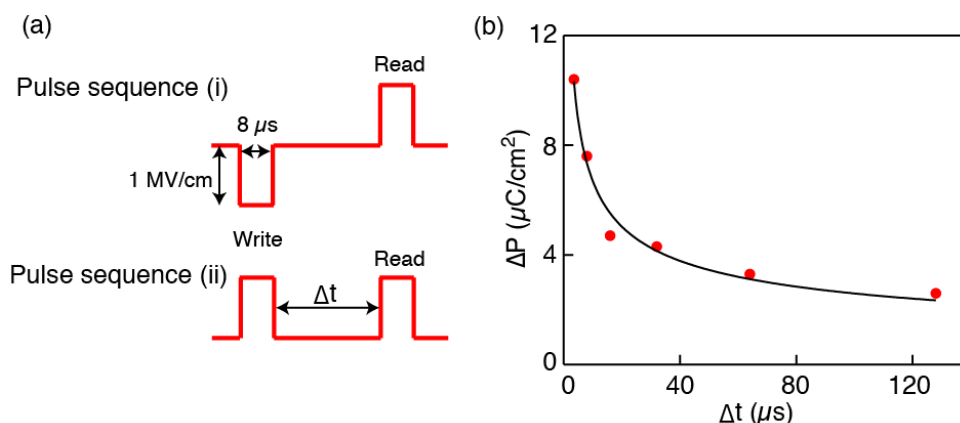


Figure 3. (a) Electric-field pulses used for polarization relaxation measurements. (b) ΔP (twice the stored polarization) of SL capacitors as a function of the delay time between write and read pulses. The solid curve is a power-law fit.

q_z as time progresses during the electric field pulse. After 291 ns, the SL reaches a strain of approximately 0.035%.

Electric fields with a longer duration result in a larger lattice distortion than the 300 ns pulses. Figure 2(b) shows a map of diffracted intensities at the $m = 2$ $l = 0$ reflection during the 2.5 ms triangle-wave electric fields. The electric field gradually increases from zero to 1 MV cm^{-1} and then decreases to zero as time progresses. A comparison of the distortions at short- and long-duration electric fields with the very similar magnitudes of 0.94 and 0.96 MV cm^{-1} , respectively, is shown in figure 2(b). Longer electric fields result in an order of magnitude larger piezoelectric distortion than shorter pulses. The difference between the piezoelectric distortions at timescales of 100 ns and 1 ms implies that a dynamical phenomenon that allows the SLs to reach the high-strain state under electric fields occurs at an intermediate characteristic time.

The timescales associated with the relaxation of the remnant electrical polarization were measured using a series of electrical pulses separated by variable delays [22, 23]. These pulse sequences for the polarization decay measurement consisted of write and read pulses, i.e. the first and the second pulse in each sequence, respectively, with magnitudes of 1 MV cm^{-1} and duration of $8 \mu\text{s}$, as shown in figure 3(a). The electrical current during these pulses was measured using a 50Ω resistor in series with the SL capacitor and integrated to obtain the switched and unswitched polarizations, (i) P_{SW} and (ii) P_{NSW} . The difference between these two polarizations is $\Delta P = P_{\text{SW}} - P_{\text{NSW}}$. For materials in which there is no decay of the polarization ΔP is time independent and has a magnitude equal to twice the remnant polarization. When the polarization relaxes during the time interval Δt between pulses, ΔP decays as Δt increases.

In the BTO/CTO SL, ΔP is a rapidly varying function of Δt , as shown in figure 3(b), indicating that there is a rapid relaxation of the polarization written by the first pulses in the sequence. ΔP is $10 \mu\text{C cm}^{-2}$ at the shortest Δt measured, where $\Delta t = 3.5 \mu\text{s}$, and decays over several tens of microseconds, reaching a steady-state value of approximately $3 \mu\text{C cm}^{-2}$ within $100 \mu\text{s}$. A rapid decay of the polarization is also reported in fatigued ferroelectric thin films and in ultrathin ferroelectric layers [22, 23]. The initial rate of decay qualitatively fits with the power-law description of Kang *et al* [22], in which $\Delta P \propto \Delta t^{-p}$. The fit shown in figure 3(b)

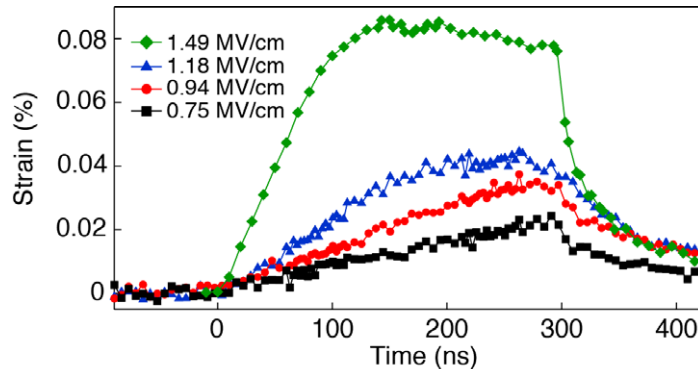


Figure 4. Strain as a function of the time during 300 ns-duration electric field pulses with magnitudes ranging from 0.75 to 1.49 MV cm⁻¹. The electric fields start at 0 ns.

corresponds to $p = 0.4$. This value of p is larger than $p = 0.23$ observed in fatigued thin films with poor retention properties [22], suggesting either effectively large depolarization electric fields or other significant driving forces returning the system to a macroscopically unpolarized state. A depolarization field of 0.06 MV cm⁻¹, for example, has been reported in SLs with different compositions [8]. We also note that the effective long-term polarization of 1.5 $\mu\text{C cm}^{-2}$ (half of ΔP) is far less than the value of 34 $\mu\text{C cm}^{-2}$ that has been previously predicted for this material in density functional theory (DFT) calculations [11]. A separate DFT calculation predicts that the spontaneous polarization of SLs can be suppressed when taking the octahedral tilt into account [10]. The small net polarization predicted in [10] is consistent with the small piezoelectric response observed under 300 ns pulses in figure 2.

4. Scaling of strain with the applied electric field

Short-duration electric field pulses lead to a dramatically different scaling of the strain with the magnitude of the electric field, compared to what has been previously observed with long-duration electric fields [12]. The piezoelectric strain as a function of time during 300 ns pulses with a wide range of electric field magnitudes is shown in figure 4. The strain in figure 4 is measured relative to the zero-field state using the average lattice constant estimated from the center of mass of diffraction patterns along the q_z direction. The strain continuously increases throughout the duration of the pulses for electric fields with magnitudes less than 1.2 MV cm⁻¹. At electric fields higher than 1.2 MV cm⁻¹, however, the strain reaches a plateau beginning at 120 ns, and can in some cases exhibit a small decrease.

A comparison of the strain measured during 300 ns pulses and 2.5 ms triangle-wave electric fields is shown in figure 5. The strain in long-duration electric fields can be separated into a nonlinear region at fields lower than 0.2 MV cm⁻¹ and a linear region at fields higher than 0.2 MV cm⁻¹. A fit to the linear region yields a piezoelectric coefficient of 36 pm V⁻¹. The strain under 300 ns electric pulses varies significantly as a function of the elapsed time, as illustrated in figure 4. Systematic analysis of the dependence of the strain on the magnitude of the electric field is conducted using values of the strain measured 250 ns after the start of the electric field pulse, where the strain is close to its maximum. The strain measured within 300 ns electric pulses is much smaller than the value anticipated using the piezoelectric coefficient

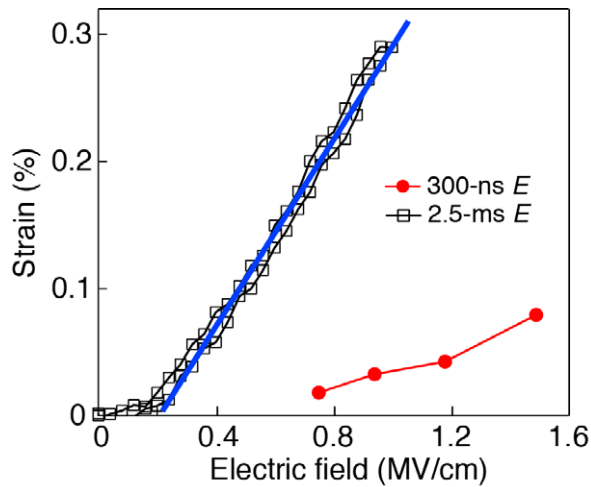


Figure 5. Strain as a function of electric field at the elapsed time of 250 ns under 300 ns pulses (circles), compared with the strain during 2.5 ms triangle-wave electric fields (squares). The blue line is a linear fit to the strain-field curve with 2.5 ms duration at fields higher than 0.2 MV cm^{-1} .

of 36 pm V^{-1} , at electric fields ranging from 0.75 to 1.49 MV cm^{-1} . For example, at electric fields of 1.49 MV cm^{-1} , we predict a strain of 0.53% using the long-duration piezoelectric coefficients, but the measured strain in 300 ns pulses is just 0.08% .

In the nonlinear low-electric-field region in the strain-field curve under long-duration electric fields, the piezoelectric distortion is 0.01% or less, much lower than the strain estimated from the piezoelectric coefficient of 36 pm V^{-1} . This low-strain regime with electric fields lower than 0.2 MV cm^{-1} continues for approximately $250 \mu\text{s}$. The reduced piezoelectric response at this initial stage of long-duration electric fields is similar to the case with 300 ns electric pulses, and is consistent with the intermediate-timescale dynamics of SLs.

The strain-field curve under long-duration electric fields exhibits no hysteresis. In a compositionally uniform ferroelectric, the polarization after the initial poling is preserved upon removal of electric fields. If this were the case in BTO/CTO SLs, one would expect a linear piezoelectric response during the decrease of electric fields from 1 MV cm^{-1} to zero. However, when the electric fields decrease to lower than 0.2 MV cm^{-1} , the piezoelectric distortion deviates from the linear curve and is again significantly reduced, as in the initial stages of long-duration electric field waveforms. This lack of hysteresis indicates that the high-field state, in which the large piezoelectric coefficient of 36 pm V^{-1} is observed, is only stable under electric fields higher than 0.2 MV cm^{-1} .

Further insight into the field-driven transition between zero-field and high-field states is obtained in electrical measurements of the capacitance of the SL as a function of electric field. The capacitance measurement was carried out using a sinusoidal electric field with a root-mean-squared amplitude of 0.05 MV cm^{-1} and a frequency of 100 kHz superimposed on the slowly varying offset electric field. The offset voltage was swept from -25 to 25 V , with a step size of 1 V , at approximately 1 s per step. The dielectric constant was calculated from the measured capacitance using the nominal thickness of 200 nm and the diameter of the capacitor of $100 \mu\text{m}$.

The field dependence of the dielectric capacitance and the computed dielectric constant is shown in figure 6. The capacitance at zero field is 170 pF and rapidly decreases at fields higher

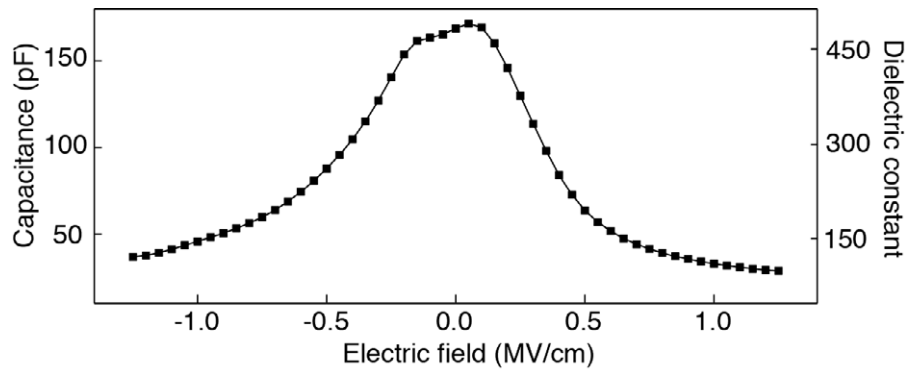


Figure 6. Capacitance and the calculated dielectric constant of the BTO/CTO SL as a function of the slowly varying component of the electric field.

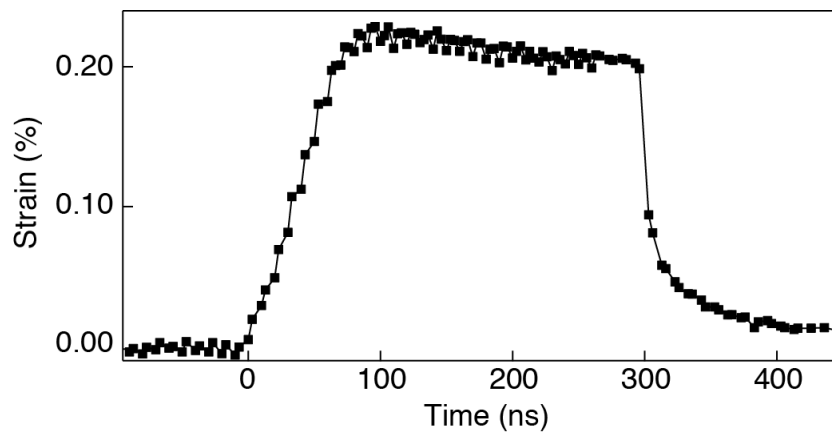


Figure 7. Strain as a function of time during 300 ns electric-field pulses with a magnitude of 2.24 MV cm^{-1} , starting at 0 ns.

than 0.1 MV cm^{-1} , reaching approximately 30 pF at 1.0 MV cm^{-1} . In addition to the decrease at high fields, figure 6 shows that the SL has a maximum capacitance near 0.1 MV cm^{-1} , at a value 4% higher than the zero-field capacitance. In other systems, a large dielectric constant at low electric fields has possible origins including both the domain switching [24] and transitions between phases of different polarization [25]. The region of electric fields where the dielectric constant is relatively large qualitatively agrees with the region where the piezoelectric distortion is reduced, as observed in figure 5 under long-duration electric fields. This similarity implies that the two phenomena, i.e. the large dielectric constant and reduced piezoelectric distortion at low fields, share the same origins.

Electric fields larger than the 1.49 MV cm^{-1} maximum of the fields in figure 4 lead to larger strains but also produce irreversible degradation of the SLs. At 2.24 MV cm^{-1} (figure 7) the piezoelectric distortion reaches a peak strain of over 0.2%. This 0.2% strain, however, is still much smaller than the 0.8% that would be obtained using the long-duration piezoelectric coefficient of 36 pm V^{-1} . At these strong fields, large variations in the piezoelectric strain among different SL capacitors were observed as a consequence of sample degradation.

5. Origins of reduced piezoelectricity

The intrinsic piezoelectric response in complex-oxide ferroelectrics occurs in times far less than 1 ns [26], and is therefore irrelevant in the intermediate-timescale dynamics discussed here. Two physical processes present possible origins of the piezoelectric behavior of the BTO/CTO SL. The first possibility is that domain dynamics limit the speed of the structural response. We note that a zero-field domain pattern has not been reported in microscopy or diffraction studies of BTO/CTO SLs. In this case, we suspect that BTO/CTO SLs form nanodomains with sufficient randomness in periodicity that their diffraction signature is below the background arising from diffuse scattering [8]. In this nanodomain picture, the applied electric field favors the polarization state parallel to the field direction and induces transitions from nanodomains into a uniform polarization state. In the zero-field unswitched SL, the piezoelectric response is suppressed by the electromechanical clamping from neighboring domains with opposite polarizations [27]. Only when a certain portion of the SL is switched can the SL be liberated from this clamping effect. The separation between 300 ns electric pulses is long enough for the SL to return to the nanodomain state, thus causing the SL to alternate between the nanodomain state and the partially poled state during the measurement. In this domain-dominated case, the difference between long- and short-timescale responses corresponds intuitively to the existence of a characteristic timescale for switching, as in single-crystal bulk ferroelectrics [28, 29].

In a previous study of PTO/STO SLs where well-defined striped nanodomains are formed, the SL was freed from this clamping effect at times much less than 100 ns, and exhibited a piezoelectric coefficient of 36 pm V^{-1} in nanosecond pulses [6]. The long, microsecond-scale timescales associated with the BTO/CTO system are thus puzzling, suggesting that the nanodomain-switching model does not apply equally well to the BTO/CTO SL.

A second possible origin of the reduced piezoelectricity at short times is that there is an electric-field-induced crystallographic symmetry transition in the BTO/CTO SL. We propose here that a phase transition driven by the electric field may induce a change from an initially less-polar state with lower symmetry to a more-polar state with higher symmetry. Transitions from non-polar to polar states have been reported in PbZrO_3 -based antiferroelectrics and rare-earth-substituted BiFeO_3 in applied electric fields [17, 30]. In the case of the BTO/CTO SL, the competition between the ferroelectric order in BTO and the non-polar antiferrodistortive order in CTO is expected to determine the equilibrium structure. Electric-field-induced antiferrodistortive-to-ferroelectric transitions in $\text{PbTiO}_3/\text{SrTiO}_3$ and BTO/CTO have been theoretically studied and linked to enhancements in piezoelectricity [13]. DFT calculations utilizing the tetragonal $P4mm$ symmetry [11] predict a piezoelectric coefficient of 51 pm V^{-1} , in agreement with our previous measurements using 2.5 ms electric fields with a magnitude of 1.25 MV cm^{-1} [12]. The large piezoelectric coefficient at long times in the BTO/CTO system is linked to the large continuous polarization throughout the entire thickness of the SL. DFT calculations have also shown that the tetragonal symmetry of the SL is unstable at zero applied field and that the distorted ground state will include rotations of oxygen octahedra in the CTO layers [10, 11]. The rotation of the oxygen octahedral predicted in [10, 11] reflects the development of antiferrodistortive order. This distortion lowers the crystallographic symmetry of the SL and reduces the ferroelectric polarization as a consequence of the competition between antiferrodistortive and ferroelectric symmetries [10]. One can therefore expect a lower piezoelectric coefficient in the distorted low-symmetry state. Electric

fields favor the ferroelectric order and are likely to stabilize the tetragonal phase with the large piezoelectric coefficient.

Little is known about the characteristic time of the field-induced phase transitions involving the competitions between antiferrodistortive and ferroelectric orders. The analogous phase transition from antiferroelectric to ferroelectric phases in PbZrO_3 -based ceramics occurs on the order of $1 \mu\text{s}$ [16], which falls in the microsecond timescale window we observed in BTO/CTO SLs. The systems and experimental methods are sufficiently different, however, that we cannot attempt a more precise comparison. In particular, the scaling of the timescale with electric fields in these phase transitions is unknown. We would like to point out, however, that the dynamics in BTO/CTO SLs requires times approaching $100 \mu\text{s}$ at low fields, which remains puzzling in this phase transition picture.

6. Conclusion

Electric fields induce dynamical processes in BTO/CTO ferroelectric/dielectric SLs and lead to piezoelectric behaviors that are distinct from previously studied uniform-composition ferroelectrics and SLs. The reduced piezoelectricity and the retention of the stored polarization reveal an intermediate-timescale dynamical phenomenon under applied electric fields. Potential origins of this effect are the polarization switching of nanodomains to a uniform polarization state or a symmetry transition from a less-polar to a more-polar state mediated by the competition between antiferrodistortive and ferroelectric orders. The nanodomain hypothesis would require extremely slow nanodomain dynamics, far slower than the previously studied PTO/STO system [6]. The reduced piezoelectricity under nanosecond pulses persists even at high electric fields, which is again inconsistent with the rapid scaling of the domain switching with electric fields observed in PTO/STO SLs [6]. Taken together, these timescales suggest that the BTO/CTO system is driven between metastable crystallographic states by a field-induced structural transition.

Acknowledgments

This work was supported by the US Department of Energy, Office of Basic Energy Sciences, Division of Materials Sciences and Engineering under award number DE-FG02-10ER46147 and contract number DE-AC05-00OR22725 (to HNL). JYJ acknowledges support from the National Research Foundation of Korea via MEST (grant numbers 2011-0009968 and 220-2011-1-C00016). SMN, EMD and the use of the Advanced Photon Source were supported by the US Department of Energy, Office of Science, Office of Basic Energy Sciences under contract number DE-AC02-06CH11357.

References

- [1] Neaton J B and Rabe K M 2003 *Appl. Phys. Lett.* **82** 1586–8
- [2] Nakhmanson S M, Rabe K M and Vanderbilt D 2005 *Appl. Phys. Lett.* **87** 102906
- [3] Tenne D A *et al* 2006 *Science* **313** 1614–6
- [4] Zubko P, Stucki N, Lichtensteiger C and Triscone J M 2010 *Phys. Rev. Lett.* **104** 187601
- [5] Lisenkov S, Ponomareva I and Bellaiche L 2009 *Phys. Rev. B* **79** 024101

- [6] Jo J Y, Chen P, Sichel R J, Callori S J, Sinsheimer J, Dufresne E M, Dawber M and Evans P G 2011 *Phys. Rev. Lett.* **107** 055501
- [7] Bousquet E, Dawber M, Stucki N, Lichtensteiger C, Hermet P, Gariglio S, Triscone J M and Ghosez P 2008 *Nature* **452** 732–6
- [8] Kathan-Galipeau K, Wu P P, Li Y L, Chen L Q, Soukiassian A, Xi X X, Schlom D G and Bonnell D A 2011 *ACS Nano* **5** 640–6
- [9] Zhong W and Vanderbilt D 1995 *Phys. Rev. Lett.* **74** 2587–90
- [10] Wu X, Rabe K M and Vanderbilt D 2011 *Phys. Rev. B* **83** 020104
- [11] Jo J Y, Sichel R J, Dufresne E M, Lee H N, Nakhmanson S M and Evans P G 2010 *Phys. Rev. B* **82** 174116
- [12] Jo J Y, Sichel R J, Lee H N, Nakhmanson S M, Dufresne E M and Evans P G 2010 *Phys. Rev. Lett.* **104** 207601
- [13] Swartz C and Wu X 2011 arXiv:1109.2183
- [14] Fu H X and Cohen R E 2000 *Nature* **403** 281–3
- [15] Zeches R J *et al* 2009 *Science* **326** 977–80
- [16] Pan W, Zhang Q, Bhalla A and Cross L E 1989 *J. Am. Ceram. Soc.* **72** 571–8
- [17] Frederick J, Tan X and Jo W 2011 *J. Am. Ceram. Soc.* **94** 1149–55
- [18] Tan X, Frederick J, Ma C, Jo W and Rodel J 2010 *Phys. Rev. Lett.* **105** 255702
- [19] Glazer A M 1972 *Acta Crystallogr. B* **28** 3384–92
- [20] Grigoriev A, Sichel R, Lee H N, Landahl E C, Adams B W, Dufresne E M and Evans P G 2008 *Phys. Rev. Lett.* **100** 027604
- [21] Seo S S A and Lee H N 2009 *Appl. Phys. Lett.* **94** 232904
- [22] Kang B S, Yoon J G, Noh T W, Song T K, Seo S, Lee Y K and Lee J K 2003 *Appl. Phys. Lett.* **82** 248–50
- [23] Kim D J, Jo J Y, Kim Y S, Chang Y J, Lee J S, Yoon J G, Song T K and Noh T W 2005 *Phys. Rev. Lett.* **95** 237602
- [24] Chai F K, Brews J R, Schrimpf R D and Birnie D P 1997 *J. Appl. Phys.* **82** 2505–16
- [25] Iwata M and Ishibashi Y 2005 *Japan. J. Appl. Phys.* **1** **44** 3095–8
- [26] Grigoriev A, Do D H, Kim D M, Eom C B, Evans P G, Adams B and Dufresne E M 2006 *Appl. Phys. Lett.* **89** 021109
- [27] Chen L and Roytburd A L 2007 *Appl. Phys. Lett.* **90** 102903
- [28] Merz W J 1954 *Phys. Rev.* **95** 690–8
- [29] Wieder H H 1957 *J. Appl. Phys.* **28** 367–9
- [30] Kan D, Palova L, Anbusathaiah V, Cheng C J, Fujino S, Nagarajan V, Rabe K M and Takeuchi I 2010 *Adv. Funct. Mater.* **20** 1108–15